CODEN IEJMAT *Internet Electronic Journal of Molecular Design* **2005**, *4*, 94–105 ISSN 1538–6414
BioChem Press http://www.biochempress.com

Inter*net* Electronic Journal of Molecular Design

February 2005, Volume 4, Number 2, Pages 94–105

Editor: Ovidiu Ivanciuc

Proceedings of the Internet Electronic Conference of Molecular Design, IECMD 2004
November 29 – December 12, 2004

Density Functional Study on the Highest and Lowest Spin States of $[Mn_2O_2(H_2O)_8]^{q+}$ (q = 0, 2, 4)

Masaki Mitani, Takeharu Katsurada, Yohei Wakamatsu, and Yasunori Yoshioka

Chemistry Department for Materials, Faculty of Engineering, Mie University, Kamihama, Tsu, Mie 514–8507, Japan

Received: October 28, 2004; Revised: January 28, 2005; Accepted: January 31, 2005; Published: February 28, 2005

Citation of the article:
M. Mitani, T. Katsurada, Y. Wakamatsu, and Y. Yoshioka, Density Functional Study on the Highest and Lowest Spin States of $[Mn_2O_2(H_2O)_8]^{q+}$ (q = 0, 2, 4), *Internet Electron. J. Mol. Des.* **2005**, *4*, 94–105, http://www.biochempress.com.

Inter*net* Electronic Journal of Molecular Design

BioChem Press
http://www.biochempress.com

Density Functional Study on the Highest and Lowest Spin States of $[Mn_2O_2(H_2O)_8]^{q+}$ (q = 0, 2, 4)

Masaki Mitani,* Takeharu Katsurada, Yohei Wakamatsu, and Yasunori Yoshioka *

Chemistry Department for Materials, Faculty of Engineering, Mie University, Kamihama, Tsu, Mie 514–8507, Japan

Received: October 28, 2004; Revised: January 28, 2005; Accepted: January 31, 2005; Published: February 28, 2005

Internet Electron. J. Mol. Des. **2005**, *4* (2), 94–105

Abstract

Motivation. Water oxidation mechanism of oxygen–evolving complex (OEC) in photosystem II (PSII) has not been established yet. Recently, the X–ray structure of PSII has been reported and it has been suggested that OEC contains cubane–like Mn_3CaO_4 cluster linked to Mn by mono–μ–oxo bridge. The Mn–Mn and Mn–Ca in cubane–like cluster are connected by di–μ–oxo bridge to form a face of cubane–like structure. As the first step to examine the mechanism of dioxygen generation by OEC, the geometrical and electronic structures of model complexes $[Mn_2O_2(H_2O)_8]^{q+}$ (q = 0, 2, 4) are investigated for the highest and lowest spin configurations from theoretical viewpoint in this work.

Method. Model complexes were constructed by placing eight H_2O molecules as ligands around Mn–Mn core with di–μ–oxo bridges to form six–coordinated Mn sites. Full geometry optimizations were carried out by the hybrid–type DFT method with B3LYP functional. For Mn, the LanL2DZ basis set with double–zeta quality was used and the effective core potential was applied. The unrestricted and broken–symmetry wave functions were obtained for the highest and lowest spin states, respectively.

Results. The coordinated positions of H_2O molecules in Mn(II)–Mn(II) complex are different from those in Mn(III)–Mn(III) or Mn(IV)–Mn(IV) complex, while Mn(III)–Mn(III) and Mn(IV)–Mn(IV) complexes have similar coordination pattern. In Mn–Mn core connected by di–μ–oxo bridges, the spin densities are well localized on Mn, and the antiferromagnetic coupling is more stable than the ferromagnetic coupling by 0.46, 5.90, and 2.58 kcal/mol for Mn(II)–Mn(II), Mn(III)–Mn(III), and Mn(IV)–Mn(IV) oxidation states, respectively.

Conclusions. The two–electron or four–electron oxidations of di–μ–oxo–bridged Mn–Mn complex occur from octahedral "e_g" orbitals of Mn.

Keywords. Photosystem II; oxygen–evolving complex; μ–oxo bridge; manganese complex; DFT; B3LYP.

1 INTRODUCTION

Photosynthetic water oxidation takes place at tetranuclear Mn cluster in photosystem II (PSII), and the functional unit including Mn cluster is referred to as oxygen–evolving complex (OEC) or water–oxidizing complex (WOC). The OEC oxidizes two water molecules to oxygen molecule at

Presented in part at the Internet Electronic Conference of Molecular Design 2004, IECMD 2004.

* Correspondence authors; M. M.: phone: 81–59–231–9256; fax: 81–59–231–9742; E–mail: mitani@chem.mie–u.ac.jp. Y. Y.: phone: 81–59–231–9742; fax: 81–59–231–9742; E–mail: yyoshi@chem.mie–u.ac.jp.

the active site of Mn cluster as $2H_2O \rightarrow O_2 + 4e^- + 4H^+$. The several reaction mechanisms of water oxidation and molecular structures of OEC have been proposed by experimental and theoretical studies until now, and the many related articles have been published (for examples, see Refs. [1–17] and references therein).

The oxidation reaction of water molecule proceeds through the S–state catalytic cycle which is the five–step oxidation from S_0 to S_4 states, and the electrons and protons are released in this cycle as shown in Figure 1 [1]. In the S–state catalytic cycle, it has been suggested that each of the S states contains the following oxidized Mn cluster: Mn(II), Mn (III), Mn(IV), and Mn(IV) for S_0 state; Mn(III), Mn(III), Mn(IV), and Mn(IV) for S_1 state; Mn(III), Mn(IV), Mn(IV), and Mn(IV) for S_2 state; Mn(III), Mn(IV), Mn(IV), and Mn(IV) plus μ–oxo radical for S_3 state; Mn(III), Mn(IV), Mn(IV), and Mn(IV) for S_4 state. Based on extended X–ray absorption fine structure (EXAFS) and electron spin echo envelope modulation (ESEEM) spectroscopy, it has been proposed that the first shell ligands of Mn are mostly oxygens, one or two nitrogens, and possibly one Cl. From the theoretical viewpoint, several models or synthetic compounds of Mn complexes with μ–oxo bridges have been studied by quantum chemical calculations in relation to Mn cluster of OEC [18–25]. However, the details of water oxidation steps by OEC in PSII have not been established yet.

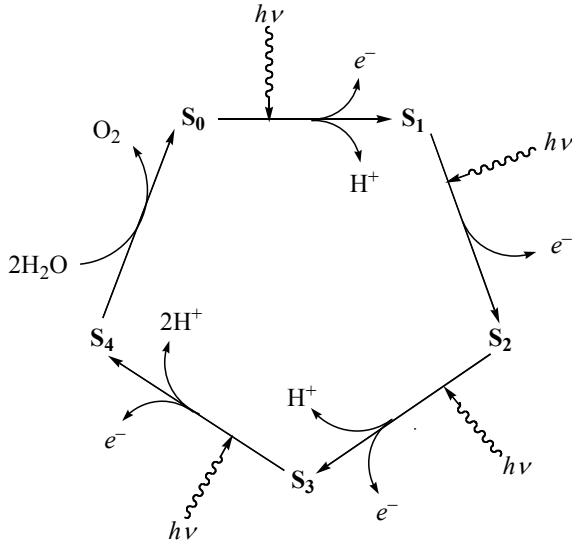

Figure 1. S–state catalytic cycle of water oxidation by OEC.

Recently, three X–ray crystallographic studies of PSII have been carried out and the three dimensional structures have been reported in Protein Data Bank (PDB) [26–28]. The two earlier crystal structures from *Synechococcus elongatus* at 3.8 Å resolution [26] and *Thermosynechococcus vulcanus* at 3.7 Å resolution [27] suggested the Y–shape Mn cluster, in which Ca was not detected. On the other hand, the newest crystal structure from *Thermosynechococcus elongatus* at 3.5 Å resolution [28] strongly indicates that the Mn cluster is cubane–like Mn_3CaO_4, in which each metal ion has tri–μ–oxo bridges, linked to Mn by mono–μ–oxo bridge. The observed X–ray structure

(PDB ID: 1S5L) is shown in Figure 2. The metal–to–metal distances were reported as about 2.7 Å for Mn–Mn and about 3.4 Å for Mn–Ca within cubane–like cluster and as about 3.3 Å for Mn–Mn between the fourth ion and the cubane–like cluster, and the details of surrounding coordination sphere around Mn cluster was also assigned. Thus, the water oxidation mechanism by Mn active site should be examined by using the X–ray structure of cubane–like Mn cluster in OEC.

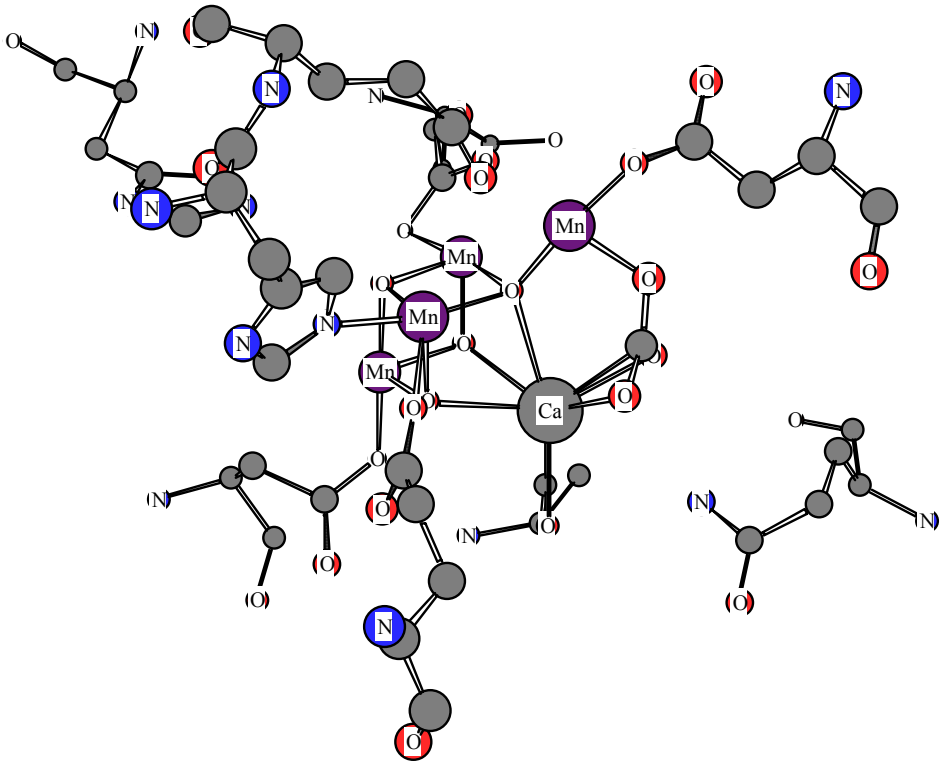

Figure 2. X–ray structure of cubane–like Mn cluster in OEC.

In this work, we investigate the geometrical and electronic structures of model complexes $[Mn_2O_2(H_2O)_8]^{q+}$ (q = 0, 2, 4) by density functional theory (DFT) as the first step toward the theoretical examination of reaction mechanism for the water oxidation by OEC, because μ–oxo–bridged Mn_2O_2 forms a face of cubane–like Mn cluster in OEC and it has been considered that only two of the four Mn sites may be sensitive to photooxidation reaction of water molecule in many of earlier models. The geometries of the highest and lowest spin states are fully optimized and the relative stability is examined. It is shown that the coordination pattern of H_2O molecules changes according to the oxidation states of Mn–Mn core and the antiferromagnetic coupling is energetically more stable than the ferromagnetic coupling.

2 MODELS AND METHODS

2.1 Model Complex

We study the binuclear Mn complexes bridged by di–μ–oxo $[Mn_2O_2(H_2O)_8]^{q+}$ (q = 0, 2, 4) shown in Figure 3 as a simplified model of tetranuclear Mn cluster in OEC. Eight H_2O molecules

were placed around Mn as ligands to form six–coordinated Mn sites. Formal charges of Mn and O are respectively taken as 2+, 3+, and 4+ and as 2–, and total charge q is 0 for Mn(II)–Mn(II) (**1**), 2 for Mn(III)–Mn(III) (**2**), and 4 for Mn(IV)–Mn(IV) (**3**) complexes. The mixed–valence states such as Mn(II)–Mn(III) or Mn(III)–Mn(IV) with q = 1 or 3 are possible in Mn complexes, and we will report the results of mixed–valence complexes elsewhere. In this paper, we take the Mn–Mn and O–O axes as the z and x axes, respectively.

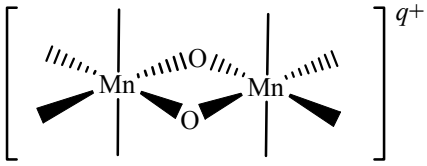

Figure 3. Model complex of Mn cluster in OEC.

We consider the equivalent oxidation of two Mn sites to satisfy the highest and lowest spin coupling with locally parallel alignment at each Mn. The 3d electron occupation is thus open shell as $(3d)^5$ for Mn(II), $(3d)^4$ for Mn(III), and $(3d)^3$ for Mn(IV), and the parallel spins on each Mn are ferromagnetically and antiferromagnetically coupled, respectively, in the highest and lowest spin states. The model complexes have total spin S of 10/2 for **1**, 8/2 for **2**, and 6/2 for **3** in the highest spin states while total spin S is 0/2 in all of the lowest spin states.

2.2 Computational Method

The electronic structure calculations were carried out at the unrestricted hybrid–type DFT level with B3LYP exchange–correlation functional [29, 30] (UB3LYP), and the molecular geometries were fully optimized without any spatial symmetry constraints. We employed LanL2DZ [31] and 6–31G(d) [32] as the basis set for Mn and for O and H, respectively, and the corresponding effective core potential (ECP) calculations were performed. The lowest spin states (S = 0/2) were obtained as the broken–symmetry solutions. All results given in this work were calculated by using Gaussian 98 program package [33].

3 RESULTS AND DISCUSSION

We show the optimized geometries of the lowest spin states in Figures 4(a) for **1**, 4(b) for **2**, and 4(c) for **3**. It is noted that the shape of Mn_2O_2 cluster and the position of H_2O molecules are similar in the highest and lowest spin states. The stable structures of **1**, **2**, and **3** satisfy C_2 symmetry around each of the x, y, or z axis approximately. As seen in Figures 4(a)–4(c), the coordinated positions of H_2O molecules are significantly different between **1** and **2** or **3**. As for **1**, O atom in H_2O molecule coordinates to Mn while one of H atoms in H_2O molecule makes hydrogen binding with μ–oxo, and H_2O molecules seem to coordinate to μ–oxo rather than Mn by hydrogen bondings. On the other

hand, H_2O molecule coordinates to Mn without hydrogen bonding with μ–oxo as for **2** and **3**.

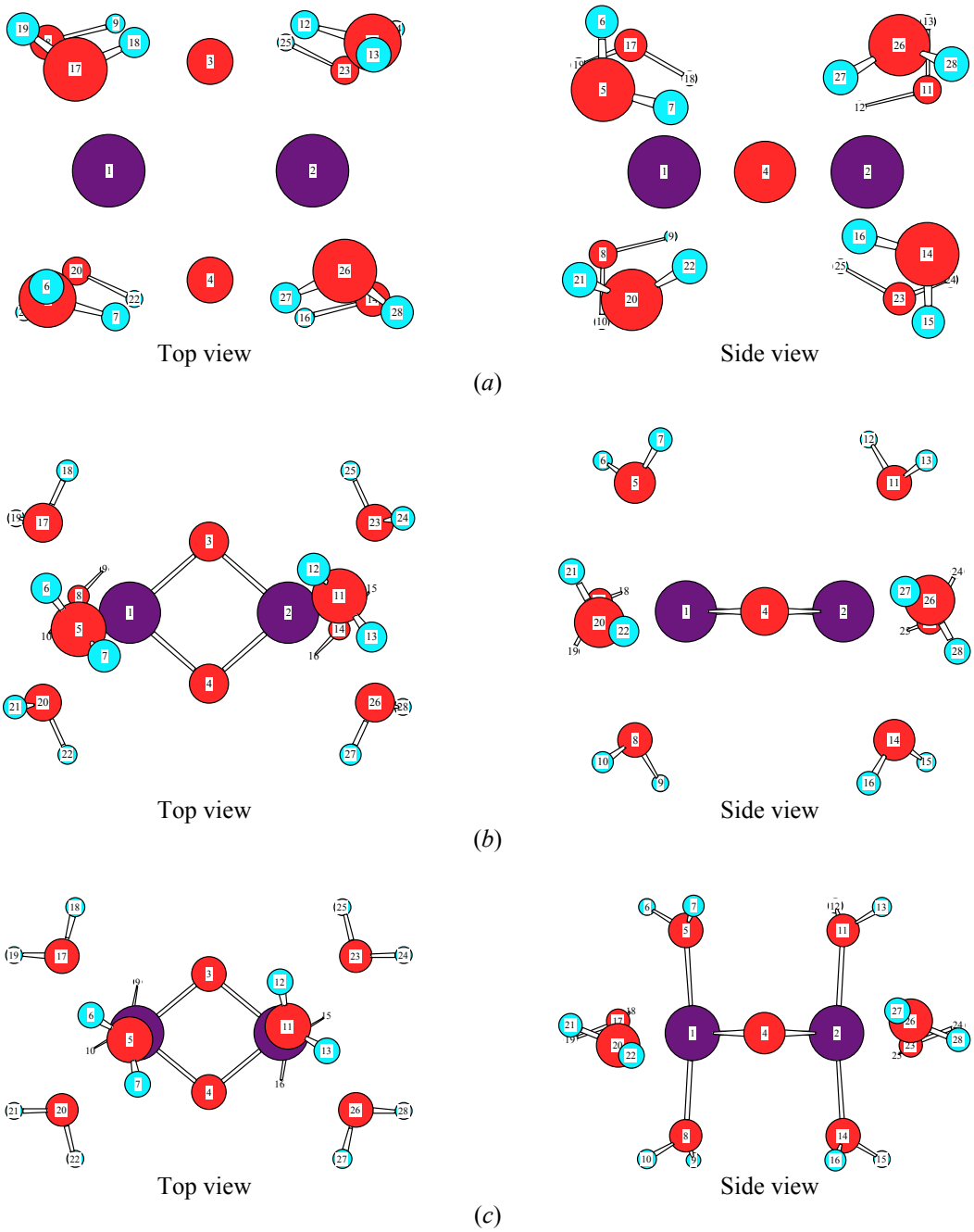

Figure 4. Optimized geometries of $[Mn_2O_2(H_2O)_8]^{q+}$ for (a) **1**, (b) **2**, and (c) **3** with numbering of atoms.

Tables 1–3 summarize the optimized geometrical parameters for Mn_2O_2 (Tables 1 and 2) and $Mn_2(H_2O)_8$ (Table 3) parts in model complexes. Table 1 also includes the Mn_2O_2 distances for $[Mn_2O_2(NH_3)_6(H_2O)_2]^{q+}$ reported in Refs. [22] and [25]. We note that the optimized molecular plane formed by Mn and μ–oxo is kept to be planar.

Table 1. Optimized interatomic distances for Mn_2O_2 in model complexes

Complex	Mn core	Total spin	Interatomic distance (Å)					
			Mn1–Mn2	O3–O4	Mn1–O3	Mn1–O4	Mn2–O3	Mn2–O4
1	II–II	S = 10/2	2.924	3.027	2.105	2.104	2.103	2.105
		S = 0/2	2.861	3.064	2.095	2.096	2.097	2.096
2	III–III	S = 8/2	2.711	2.416	1.816	1.816	1.816	1.816
		S = 0/2	2.696	2.397	1.804	1.804	1.804	1.804
3	IV–IV	S = 6/2	2.766	2.307	1.800	1.800	1.800	1.800
		S = 0/2	2.776	2.255	1.788	1.788	1.788	1.788
Ref. [22] [a]	III–III	S = 8/2	2.810	2.452	1.865	1.865	1.865	1.865
		S = 0/2	2.791	2.433	1.852	1.852	1.852	1.852
	IV–IV	S = 6/2	2.941	2.318	1.873	1.873	1.873	1.873
		S = 0/2	2.902	2.283	1.846	1.846	1.846	1.846
Ref. [25] [b]	III–III	S = 8/2	2.747	2.474	1.831	1.866	1.866	1.831
		S = 0/2	2.710	2.441	1.804	1.843	1.843	1.804
	IV–IV	S = 6/2	2.806	2.371	1.805	1.868	1.868	1.805
		S = 0/2	2.834	2.272	1.789	1.842	1.842	1.789

[a] Results for $[Mn_2O_2(NH_3)_6(H_2O)_2]^{q+}$ are taken from Ref. [22].
[b] Results for $[Mn_2O_2(NH_3)_6(H_2O)_2]^{q+}$ are taken from Ref. [25].

Table 2. Optimized bond angles for Mn_2O_2 in model complexes

Complex	Mn core	Total spin	Bond angle (˚)			
			Mn1–O3–Mn2	Mn1–O4–Mn2	O3–Mn1–O4	O3–Mn2–O4
1	II–II	S = 10/2	88.0	88.0	92.0	92.0
		S = 0/2	86.0	86.0	93.9	93.9
2	III–III	S = 8/2	96.6	96.6	83.4	83.4
		S = 0/2	96.7	96.7	83.3	83.3
3	IV–IV	S = 6/2	100.3	100.3	79.7	79.7
		S = 0/2	101.8	101.8	78.2	78.2

Table 3. Optimized interatomic distances for $Mn_2(H_2O)_8$ in model complexes

Complex	Mn core	Total spin	Interatomic distance (Å)			
			Mn1–O5, –O8	Mn1–O17, –O20	Mn2–O11, –O14	Mn2–O23, –O26
1	II–II	S = 10/2	2.296, 2.297	2.318, 2.315	2.297, 2.297	2.315, 2.318
		S = 0/2	2.300, 2.302	2.324, 2.322	2.300, 2.302	2.321, 2.324
2	III–III	S = 8/2	2.371, 2.371	2.118, 2.118	2.371, 2.371	2.118, 2.118
		S = 0/2	2.366, 2.367	2.124, 2.124	2.367, 2.367	2.124, 2.124
3	IV–IV	S = 6/2	1.974, 1.974	2.058, 2.058	1.974, 1.974	2.058, 2.058
		S = 0/2	1.973, 1.973	2.055, 2.055	1.973, 1.973	2.055, 2.055

The interatomic distances of Mn_2O_2, especially O–O distances, are longer in **1** than in **2** or **3** as 2.924 and 2.861 Å for Mn–Mn, 3.027 and 3.064 Å for O–O, and 2.105 and 2.096 Å for Mn–O in **1**, 2.711 and 2.696 Å for Mn–Mn, 2.416 and 2.397 Å for O–O, and 1.816 and 1.804 Å for Mn–O in **2**, and 2.766 and 2.776 Å for Mn–Mn, 2.307 and 2.255 Å for O–O, and 1.800 and 1.788 Å for Mn–O in **3**. The Mn–Mn, O–O, and Mn–O bonds are thus respectively elongated by about 0.2, 0.6–0.7, and 0.3 Å in **1** than in **2** or **3**. The Mn–O–Mn angles (88.0 and 86.0˚) are slightly smaller than the O–Mn–O angles (92.0 and 93.9˚) in **1** while the Mn–O–Mn angles (96.6 and 96.7˚ for **2** or 100.3 and 101.8˚ for **3**) are larger than the O–Mn–O angles (83.4 and 83.3˚ for **2** or 79.7 and 78.2˚ for **3**) in **2** or **3**. These results indicate that the Mn_2O_2 core forms nearly square in **1** and rhombus in **2** or **3**.

Model complexes $[Mn_2O_2(NH_3)_6(H_2O)_2]^{q+}$ have been calculated by using DFT method [22, 25],

and the only interatomic distances of Mn_2O_2 have been reported as follows: Mn–Mn = 2.810 [22] and 2.747 Å [25], O–O = 2.452 [22] and 2.474 Å [25], and Mn–O = 1.865 [22], 1.831 and 1.866 Å [25] for the highest spin state of Mn(III)–Mn(III) complex; Mn–Mn = 2.791 [22] and 2.710 Å [25], O–O = 2.433 [22] and 2.441 Å [25], and Mn–O = 1.852 [22], 1.804 and 1.843 Å [25] for the broken–symmetry lowest spin state of Mn(III)–Mn(III) complex; Mn–Mn = 2.941 [22] and 2.806 Å [25], O–O = 2.318 [22] and 2.371 Å [25], and Mn–O = 1.873 [22], 1.805 and 1.868 Å [25] for the highest spin state of Mn(IV)–Mn(IV) complex; Mn–Mn = 2.902 [22] and 2.834 Å [25], O–O = 2.283 [22] and 2.272 Å [25], and Mn–O = 1.846 [22], 1.789 and 1.842 Å [25] for the broken–symmetry lowest spin state of Mn(IV)–Mn(IV) complex. From the comparison of our results with earlier results [22,25], it is found that the interatomic distances of Mn_2O_2 become slightly shorter in $[Mn_2O_2(H_2O)_8]$ than in $[Mn_2O_2(NH_3)_6(H_2O)_2]$.

The distances between Mn_2O_2 core and H_2O molecules are 2.296–2.324 Å for **1**, 2.366–2.371 and 2.118–2.124 Å for **2**, and 1.973–2.058 Å for **3**, indicating that the H_2O molecules at axial positions (O5, O8, O11, and O14) are somewhat apart from Mn than the H_2O molecules at equatorial positions (O17, O20, O23, and O26) in **2** while all of the H_2O molecules are nearly equidistant from Mn in **1** or **3**.

The relative energies of model complexes are given in Table 4, and the charge and spin densities on Mn_2O_2 core and H_2O ligands are listed in Table 5 and in Tables 6 and 7.

Table 4. Total and relative energies of model complexes

Complex	Mn core	Total spin	$<S^2>$	Total energy (a.u.)	Relative energy (kcal/mol)
1	II–II	S = 10/2	30.006	–969.87018	0.46
		S = 0/2	4.988	–969.87091	0.00
2	III–III	S = 8/2	20.117	–969.35464	5.90
		S = 0/2	4.043	–969.36404	0.00
3	IV–IV	S = 6/2	12.213	–968.08829	2.58
		S = 0/2	3.041	–968.09241	0.00

Table 5. Mulliken charge and spin densities for Mn_2O_2 in model complexes

Complex	Mn core	Total spin	Charge density				Spin density			
			Mn1	Mn2	O3	O4	Mn1	Mn2	O3	O4
1	II–II	S = 10/2	0.590	0.590	–0.943	–0.943	4.756	4.756	0.151	0.151
		S = 0/2	0.582	0.582	–0.944	–0.944	4.807	–4.807	0.000	–0.000
2	III–III	S = 8/2	1.025	1.025	–0.749	–0.750	3.890	3.890	0.061	0.061
		S = 0/2	1.015	1.015	–0.733	–0.733	3.850	–3.850	–0.000	0.000
3	IV–IV	S = 6/2	1.322	1.322	–0.579	–0.579	3.014	3.014	–0.042	–0.042
		S = 0/2	1.315	1.315	–0.576	–0.576	2.853	–2.853	0.000	–0.000

The expectation values of spin angular momentum for the lowest spin states as 5 for **1**, 4 for **2**, and 3 for **3** indicate that these states are obtained as the broken–symmetry solutions. The relative energies between the highest and lowest spin states show that the antiferromagnetic spin coupling of Mn–Mn is energetically more stable than the ferromagnetic spin coupling of Mn–Mn by 0.46 kcal/mol for **1**, 5.90 kcal/mol for **2**, and 2.58 kcal/mol for **3**. However, the energy difference

becomes small for **1**, because longer Mn–Mn distance than **2** or **3** causes the weak interactions between spins on each Mn.

Table 6. Mulliken charge densities for H_2O in model complexes [a]

Complex	Mn core	Total spin	Site1	Site2	Site3	Site4	Site5	Site6	Site7	Site8
1	II–II	S = 10/2	0.089	0.088	0.089	0.088	0.088	0.088	0.088	0.088
		S = 0/2	0.092	0.091	0.092	0.091	0.089	0.089	0.090	0.089
2	III–III	S = 8/2	0.153	0.153	0.153	0.153	0.209	0.209	0.209	0.209
		S = 0/2	0.152	0.152	0.152	0.152	0.207	0.207	0.207	0.207
3	IV–IV	S = 6/2	0.333	0.333	0.333	0.333	0.295	0.295	0.295	0.295
		S = 0/2	0.334	0.334	0.334	0.334	0.296	0.296	0.296	0.296

[a] H_2O sites are defined by site1: O5, site2: O8, site3: O11, site4: O14, site5: O17, site6: O20, site7: O23, and site7: O26.

Table 7. Mulliken spin densities for H_2O in model complexes [a]

Complex	Mn core	Total spin	Site1	Site2	Site3	Site4	Site5	Site6	Site7	Site8
1	II–II	S = 10/2	0.024	0.024	0.024	0.024	0.022	0.022	0.022	0.022
		S = 0/2	0.012	0.012	–0.012	–0.012	0.016	0.016	–0.016	–0.016
2	III–III	S = 8/2	0.026	0.026	0.026	0.026	–0.001	–0.001	–0.001	–0.001
		S = 0/2	0.025	0.025	–0.025	–0.025	0.001	0.001	–0.001	–0.001
3	IV–IV	S = 6/2	–0.005	–0.005	–0.005	–0.005	0.019	0.019	0.019	0.019
		S = 0/2	–0.011	–0.011	0.011	0.010	0.016	0.016	–0.016	–0.016

[a] H_2O sites are defined by site1: O5, site2: O8, site3: O11, site4: O14, site5: O17, site6: O20, site7: O23, and site7: O26.

The charge densities on Mn are respectively given as 0.590 and 0.582 for **1**, 1.025 and 1.015 for **2**, and 1.322 and 1.315 for **3**. These values of atomic charges seem to be too small for oxidized Mn ions, and the ECP calculations may affect the charge distributions of complexes [34]. On the other hand, the spin densities are almost localized on Mn reasonably as 4.756 and 4.807 for **1**, 3.890 and 3.850 for **2**, and 3.014 and 2.853 for **3**. The charge and spin distributions on H_2O ligands are summarized as follows: about 0.09 for **1**, about 0.15 and 0.21 for **2**, and about 0.30 and 0.33 for **3** (charge densities); about 0.02 for the highest spin state of **1**, about ±0.01 and ±0.02 for the lowest spin state of **1**, about –0.00 and 0.03 for the highest spin state of **2**, about ±0.00 and ±0.03 for the lowest spin state of **2**, about –0.01 and 0.02 for the highest spin state of **3**, and about ±0.01 and ±0.02 for the lowest spin state of **3** (spin densities), indicating that the spin populations are not distributed on H_2O molecules.

The main 3d electron configurations of singly–occupied natural orbitals, which make singlet biradical pair with 2.0 as the sum of occupation numbers, are summarized for the lowest spin states of model complexes in Table 8. It is found from Table 8 that the broken–symmetry orbitals are constructed by the in–phase or out–of–phase mixing of 3d orbitals on two Mn sites. All of the 3d orbitals in **1** with Mn(II)–Mn(II) core are occupied while 3dxz orbitals in **2** with Mn(III)–Mn(III) core or 3dxz and 3dx^2–y^2 orbitals in **3** with Mn(IV)–Mn(IV) core are unoccupied, indicating that the electrons of octahedral "e_g" orbitals are removed in Mn–Mn oxidation states.

Table 8. Main 3d electron configurations for singly–occupied natural orbitals of model complexes

Complex	Mn core	Total spin	Occupation	Configuration [a]	Occupation	Configuration [a]
1	II–II	S = 0/2	1.112	dx^2-y^2 (1) + dx^2-y^2 (2)	0.888	– dx^2-y^2 (1) + dx^2-y^2 (2)
			1.074	dxz (1) + dxz (2)	0.926	– dxz (1) + dxz (2)
			1.026	– dxy (1) + dxy (2)	0.974	dxy (1) + dxy (2)
			1.013	dyz (1) – dyz (2)	0.987	dyz (1) + dyz (2)
			1.007	dz^2 (1) + dz^2 (2)	0.993	dz^2 (1) – dz^2 (2)
2	III–III	S = 0/2	1.200	– dxy (1) + dxy (2)	0.800	dxy (1) + dxy (2)
			1.146	dx^2-y^2 (1) + dx^2-y^2 (2)	0.854	dx^2-y^2 (1) – dx^2-y^2 (2)
			1.135	dyz (1) + dyz (2)	0.865	– dyz (1) + dyz (2)
			1.125	dz^2 (1) – dz^2 (2)	0.875	dz^2 (1) + dz^2 (2)
3	IV–IV	S = 0/2	1.227	– dxy (1) + dxy (2)	0.773	dxy (1) + dxy (2)
			1.227	dyz (1) + dyz (2)	0.773	– dyz (1) + dyz (2)
			1.129	– dz^2 (1) + dz^2 (2)	0.871	dz^2 (1) + dz^2 (2)

[a] Number in parenthesis indicates the numbering of Mn.

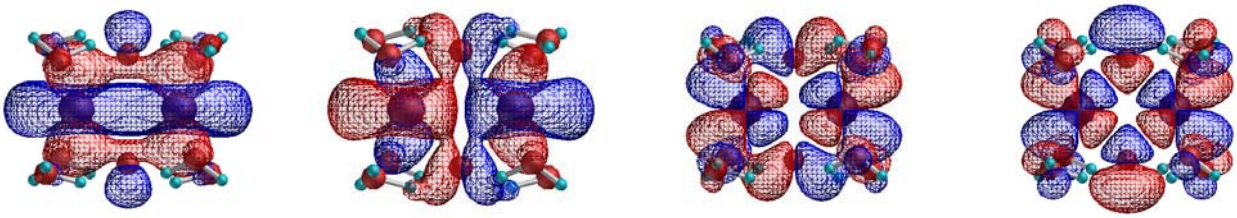

dx^2-y^2 (1) + dx^2-y^2 (2) – dx^2-y^2 (1) + dx^2-y^2 (2) dxz (1) + dxz (2) – dxz (1) + dxz (2)

Figure 5. Octahedral "e_g" orbitals of model complex **1**.

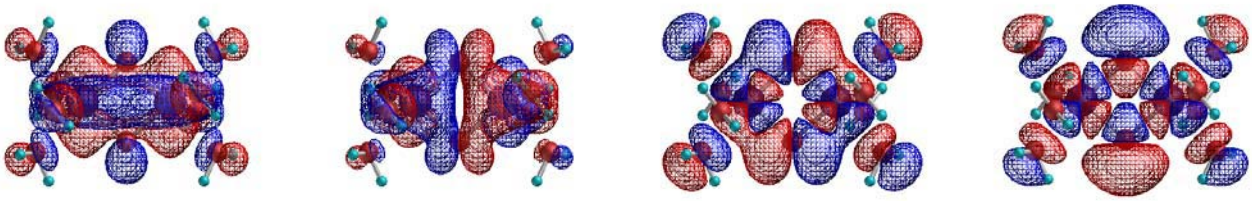

dx^2-y^2 (1) + dx^2-y^2 (2) dx^2-y^2 (1) – dx^2-y^2 (2) dxz (1) + dxz (2) – dxz (1) + dxz (2)

Figure 6. Octahedral "e_g" orbitals of model complex **2**.

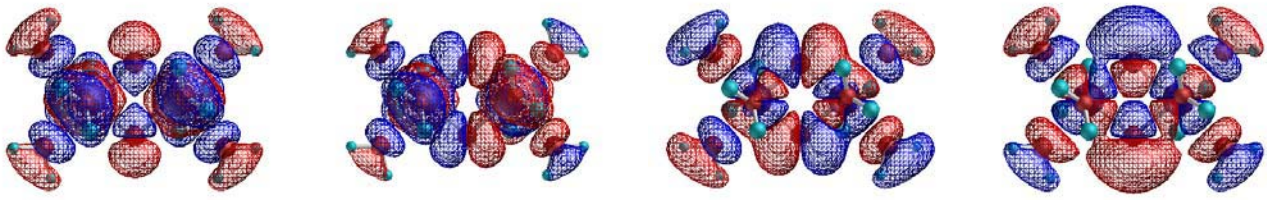

dx^2-y^2 (1) + dx^2-y^2 (2) dx^2-y^2 (1) – dx^2-y^2 (2) dxz (1) + dxz (2) – dxz (1) + dxz (2)

Figure 7. Octahedral "e_g" orbitals of model complex **3**.

We show octahedral "e_g" natural orbitals (3dx^2–y^2 and 3dxz orbitals) of the lowest spin states in Figures 5–7 for **1**, **2**, and **3**, and the number in parenthesis denotes the numbering of Mn. The 3dxz orbitals with in–phase or out–of–phase coupling between Mn–Mn are respectively interacting with 2px or 2pz orbitals of μ–oxo, which have the antibonding character as for Mn–O bonds, especially for **1**. These orbitals are occupied orbitals in **1** and unoccupied orbitals in **2** or **3**, and which may cause the long interatomic distances between Mn and μ–oxo in **1**.

4 CONCLUSIONS

We studied the stable geometries and electronic structures of model complexes $[Mn_2O_2(H_2O)_8]^{q+}$ (q = 0, 2, 4) with Mn(II)–Mn(II), Mn(III)–Mn(III), and Mn(IV)–Mn(IV) cores linked by di–μ–oxo bridges. The coordinated positions of H_2O molecules are largely different between Mn(II)–Mn(II) and Mn(III)–Mn(III) or Mn(IV)–Mn(IV) complex. The structure of Mn_2O_2 cluster changes from nearly square to rhombus shape according to the oxidation states of Mn–Mn from Mn(II)–Mn(II) to Mn(IV)–Mn(IV). The antiferromagnetically–coupled lowest spin states are more stable than the ferromagnetically–coupled highest spin states in oxidized Mn(III)–Mn(III) and Mn(IV)–Mn(IV) cores, and the spin densities are well localized on Mn in all of the Mn(II)–Mn(II), Mn(III)–Mn(III), and Mn(IV)–Mn(IV) oxidation states. In the two–electron and four–electron oxidations of Mn_2O_2 cluster from Mn(II)–Mn(II) to Mn(III)–Mn(III) and Mn(IV)–Mn(IV), the electrons which occupy the 3dxz and 3dx^2–y^2 orbitals (octahedral "e_g" orbitals) are oxidized primary and secondary.

In the S–state catalytic cycle of water oxidation by OEC, it has been considered that two of four Mn sites in tetranuclear Mn cluster keep the Mn(IV)–Mn(IV) oxidation state through S_0–S_4 states and the active site in tetranuclear Mn cluster forms the Mn(III)–Mn(III) oxidation state for S_1 state. Judging from the relative stabilities of model complexes in the present study, it is suggested that both of the oxidation states may be the low spin states with antiferromangetic Mn–Mn interaction. However, the Mn(II)–Mn(III) and Mn(III)–Mn(IV) oxidation states would be generated in the S–state catalytic cycle. Therefore, toward the theoretical examination of the oxidation mechanism, the geometrical and electronic structures (the relative stabilities, the charge and spin distributions, and the electronic configurations) should be clarified for the mixed–valence states of Mn cluster. Further works of all electron calculations using the basis set with VDZ quality are now in progress for the iso– and mixed–valence states of model complexes $[Mn_2O_2(H_2O)_8]^{q+}$. We will report the results elsewhere.

5 REFERENCES

[1] J. Messinger, Towards Understanding the Chemistry of Photosynthetic Oxygen Evolution: Dynamic Structural Changes, Redox States and Substrate Water Binding of the Mn Cluster in Photosystem II, *Biochem*. *Biophys*. *Acta* **2000**, *1459*, 481–488.

[2] P. E. M. Siegbahn, Theoretical Models for the Oxygen Radical Mechanism of Water Oxidation and of the Water

Oxidizing Complex of Photosystem II, *Inorg. Chem.* **2000**, *39*, 2923–2935.
[3] P. E. M. Siegbahn and R. H. Crabtree, Quantum Chemical Studies on Metal–Oxo Species Related to the Mechanisms of Methane Monooxygenase and Photosynthetic Oxygen Evolution, *Structure and Bonding*. **2000**, *97*, 125–144.
[4] J. H. Robblee, R. M. Cinco, and V. K. Yachandra, X–Ray Spectroscopy–Based Structure of the Mn Cluster and Mechanism of Photosynthetic Oxygen Evolution, *Biochem. Biophys. Acta* **2001**, *1503*, 7–23.
[5] H. Dau, L. Iuzzolino, and J. Dittmer, The Tetra–Manganese Complex of Photosystem II during Its Redox Cycle – X–Ray Absorption Results and Mechanistic Implications, *Biochem. Biophys. Acta* **2001**, *1503*, 24–39.
[6] J. H. A. Nugent, A. M. Rich, and M. C. W. Evans, Photosynthetic Water Oxidation: Toward A Mechanism, *Biochem. Biophys. Acta* **2001**, *1503*, 138–146.
[7] T. G. Carrell, A. M. Tyryshkin, and G. C. Dismukes, An Evaluation of Structural Models for the Photosynthetic Water–Oxidizing Complex Derived from Spectroscopic and X–Ray Diffraction Signatures, *J. Biol. Inorg. Chem.* **2002**, *7*, 2–22.
[8] J. Barber, Photosystem II: A Multisubunit Membrane Protein That Oxidises Water, *Curr. Opin. Struct. Biol.* **2002**, *12*, 523–530.
[9] P. E. M. Siegbahn, Quantum Chemical Studies of Manganese Centers in Biology, *Curr. Opin. Chem. Biol.* **2002**, *6*, 227–235.
[10] M. R. A. Blomberg and P. E. M. Siegbahn, A Quantum Chemical Study of Tyrosyl Reduction and O–O Bond Formation in Photosystem II, *Mol. Phys.* **2003**, *101*, 323–333.
[11] M. Lundberg, M. R. A. Blomberg, and P. E. M. Siegbahn, Modeling Water Exchange on Monomeric and Dimeric Mn Centers, *Theor. Chem. Acc.* **2003**, *110*, 130–143.
[12] P. E. M. Siegbahn, and M. R. A. Blomberg, Important Roles of Tyrosines in Photosystem II and Cytochrome Oxidase, *Biochem. Biophys. Acta* **2004**, *1655*, 45–50.
[13] J. Barber, Water, Water Everywhere, and Its Remarkable Chemistry, *Biochem. Biophys. Acta* **2004**, *1655*, 123–132.
[14] K. Sauer and V. K. Yachandra, The Water–Oxidation Complex in Photosystem II, *Biochem. Biophys. Acta* **2004**, *1655*, 140–148.
[15] R. D. Britt, K. A. Campbell, J. M. Peloquin, M. L. Gilchrist, C. P. Aznar, M. M. Dicus, J. Robblee, and J. Messinger, Recent Pulsed EPR Studies of the Photosystem II Oxygen–Evolving Complex: Implications as to Water Oxidation Mechanism, *Biochem. Biophys. Acta* **2004**, *1655*, 158–171.
[16] R. J. Pace and K. A. Åhrling, Water Oxidation in PSII – H Atom Abstraction Revisited, *Biochem. Biophys. Acta* **2004**, *1655*, 172–178.
[17] S. Iwata and J. Barber, Structure of Photosystem II and Molecular Architecture of the Oxygen–Evolving Center, *Curr. Opin. Struct. Biol.* **2004**, *14*, 447–453.
[18] D. M. Proserpio, R. Hoffmann, and G. C. Dismukes, Molecular Mechanism of Photosynthetic Oxygen Evolution: A Theoretical Approach, *J. Am. Chem. Soc.* **1992**, *114*, 4374–4382.
[19] X. G. Zhao, W. H. Richardson, J. –L. Chen, J. Li, L. Noodleman, H. –L. Tsai, and D. N. Hendrickson, Density Functional Calculations of Electronic Structure, Charge Distribution, and Spin Coupling in Manganese–Oxo Dimer Complexes, *Inorg. Chem.* **1997**, *36*, 1198–1217.
[20] J. E. McGrady and R. Stranger, Redox–Induced Formation and Cleavage of O–O σ and π Bonds in a Peroxo–Bridged Manganese Dimer: A Density Functional Study, *Inorg. Chem.* **1999**, *38*, 550–558.
[21] C. D. Delfs and R. Stranger, Oxidation State Dependence of the Geometry, Electronic Structure, and Magnetic Coupling in Mixed Oxo– and Carboxylato–Bridged Manganese, *Inorg. Chem.* **2001**, *40*, 3061–3076.
[22] G. Aullón, E. Ruiz, and S. Alvarez, Theoretical Clues to the Mechanism of Dioxygen Formation at the Oxygen–Evolving Complex of Photosystem II, *Chem. Eur. J.* **2002**, *8*, 2508–2515.
[23] C. D. Delfs and R. Stranger, Investigating the Stability of the Peroxide Bridge in (μ–Oxo)– and Bis(μ–Oxo)–Manganese Clusters, *Inorg. Chem.* **2003**, *42*, 2495–2503.
[24] M. Lundberg, M. R. A. Blomberg, and P. E. M. Siegbahn, Oxyl Radical Required for O–O Bond Formation in Synthetic Mn–Catalyst, *Inorg. Chem.* **2004**, *43*, 264–274.
[25] S. Petrie and R. Stranger, On the Mechanism of Dioxygen Formation from a Di–μ–Oxo–Bridged Manganese Dinuclear Complex, *Inorg. Chem.* **2004**, *43*, 5237–5244.
[26] A. Zouni, H. –T. Witt, J. Kern, P. Fromme, N. Krauβ, W. Saenger, and P. Orth, Crystal Structure of Photosystem II from *Synechococcus Elongatus* at 3.8 Å Resolution, *Nature* **2001**, *409*, 739–743.
[27] N. Kamiya and J. –R. Shen, Crystal Structure of Oxygen–Evolving Photosystem II from *Thermosynechococcus Vulcanus* at 3.7–Å Resolution, *Proc. Natl. Acad. Sci. U.S.A.* **2003**, *100*, 98–103.
[28] K. N. Ferreira, T. M. Iverson, K. Maghlaoui, J. Barber, and S. Iwata, Architecture of the Photosynthetic Oxygen–

Evolving Center, *Science* **2004**, *303*, 1831–1838.
[29] A. D. Becke, Density–Functional Thermochemistry. III. The Role of Exact Exchange, *J. Chem. Phys.* **1993**, *98*, 5648–5652.
[30] C. Lee, W. Yang, and R. G. Parr, Development of the Colle–Salvetti Correlation–Energy Formula into a Functional of the Electron Density, *Phys. Rev. B* **1988**, *37*, 785–789.
[31] P. J. Hay and W. R. Wadt, Ab Initio Effective Core Potentials for Molecular Calculations. Potentials for the Transition Metal Atoms Sc to Hg, *J. Chem. Phys.* **1985**, *82*, 270–283.
[32] P. C. Hariharan and J. A. Pople, The Influence of Polarization Function on Molecular Orbital Hydrogenation Energies, *Theor. Chim. Acta* **1973**, *28*, 213–222.
[33] Gaussian 98, Revision A.6, M. J. Frisch, G. W. Trucks, H. B. Schlegel, G. E. Scuseria, M. A. Robb, J. R. Cheeseman, V. G. Zakrzewski, J. A. Montgomery, Jr., R. E. Stratmann, J. C. Burant, S. Dapprich, J. M. Millam, A. D. Daniels, K. N. Kudin, M. C. Strain, O. Farkas, J. Tomasi, V. Barone, M. Cossi, R. Cammi, B. Mennucci, C. Pomelli, C. Adamo, S. Clifford, J. Ochterski, G. A. Petersson, P. Y. Ayala, Q. Cui, K. Morokuma, D. K. Malick, A. D. Rabuck, K. Raghavachari, J. B. Foresman, J. Cioslowski, J. V. Ortiz, B. B. Stefanov, G. Liu, A. Liashenko, P. Piskorz, I. Komaromi, R. Gomperts, R. L. Martin, D. J. Fox, T. Keith, M. A. Al–Laham, C. Y. Peng, A. Nanayakkara, C. Gonzalez, M. Challacombe, P. M. W. Gill, B. Johnson, W. Chen, M. W. Wong, J. L. Andres, C. Gonzalez, M. Head–Gordon, E. S. Replogle, and J. A. Pople, Gaussian, Inc., Pittsburgh PA, 1998.
[34] We have used the Mulliken population analysis implemented in Gaussian program package to estimate the net charges. The net charges in this study are thus simply given as the differences between nuclear charges and Mulliken atomic populations. The electron distributions of model complexes given by the interacting occupied MOs between metals and ligands are delocalized, indicating that the calculated net charges on Mn are not coincide with the formal charges and would become smaller than the formal charges. Therefore, the calculated net charges on Mn do not give the formal charges of Mn. However, the Mulliken charges on oxidized Mn using LanL2DZ basis set and ECP seems to be somewhat too small for us, especially concerning Mn(II) = 0.590 and 0.582 for the highest and lowest spin states. After the submission of this paper, all electron calculations using the basis set with VDZ quality are now in progress for the model complexes. The Mulliken population analysis of Mn(II)–Mn(II) complex shows the following charge and spin densities: Mn(II) = 1.297, O = –1.109 and –1.108, and H_2O = –0.050, –0.049 and –0.045 for the highest spin state and Mn(II) = 1.294, O = –1.111 and –1.112, and H_2O = –0.043, –0.048, and –0.049 for the lowest spin state (charge densities); Mn(II) = 4.756, O = 0.138 and 0.137, and H_2O = 0.025 and 0.029 for the highest spin state and Mn(II) = 4.754 and –4.754, O = –0.000 and 0.001, and H_2O = –0.021, –0.013, 0.013, and 0.021 for the lowest spin state (spin densities). Although the Mulliken spin densities are almost the same between the ECP and all electron calculations, the Mulliken charge densities, especially on Mn, largely depend on the computation methods with or without ECP. We will report the comparison of results between the ECP and all electron calculations elsewhere.

Biographies

Masaki Mitani is associate professor of chemistry at Mie University. After obtaining a Ph.D. degree in quantum chemistry from Hiroshima University, Dr. Mitani undertook postdoctoral research with Professor Kizashi Yamaguchi at Osaka University and Professor Ko Saito at Hiroshima University. More recently, Dr. Mitani has collaborated on reaction mechanism of enzyme and vibrational structures of small molecules with Professors Kizashi Yamaguchi and Toshio Kasai at Osaka University.

Takeharu Katsurada is graduate student of chemistry at Mie University.

Yohei Wakamatsu is student of chemistry at Mie University.

Yasunori Yoshioka is professor of chemistry at Mie University. After obtaining a Ph.D. degree in quantum chemistry from Osaka University, Dr. Yoshioka undertook postdoctoral research with Professor Kenneth D. Jordan at the University of Pittsburgh and Professor Henry F. Schaefer III at the University of California, Berkeley. More recently, Dr. Yoshioka has collaborated on reaction mechanism of enzyme and vibrational structures of small molecules with Professors Kizashi Yamaguchi and Toshio Kasai at Osaka University.